J Mol Model (2013) 19:839–846
DOI 10.1007/s00894-012-1612-z

ORIGINAL PAPER

On the influence of point defects on the structural and electronic properties of graphene-like sheets: a molecular simulation study

Ernesto Chigo Anota · Alejandro Escobedo-Morales · Martin Salazar Villanueva · Odilon Vázquez-Cuchillo · Efrain Rubio Rosas

Received: 27 June 2012 / Accepted: 26 September 2012 / Published online: 14 October 2012

Abstract The influence of vacancies and substitutional defects on the structural and electronic properties of graphene, graphene oxide, hexagonal boron nitride, and boron nitride oxide two-dimensional molecular models was studied using density functional theory (DFT) at the level of local density approximation (LDA). Bond length, dipole moment, HOMO–LUMO energy gap, and binding energy were calculated for each system with and without point defects. The results obtained indicate that the formation of a point defect does not necessary lead to structural instability; nevertheless, surface distortions and reconstruction processes were observed, mainly when a vacancy-type defect is generated. For graphene, it was found that incorporation of a point defect results in a semiconductor–semimetal transition and also increases notably its polar character. As with graphene, the formation of a point defect in a hexagonal boron nitride sheet reduces its energy gap, although its influence on the resulting dipole moment is not as dramatic as in graphene. The influence of point defects on the structural and electronic properties of graphene oxide and boron nitride oxide sheets were found to be mediated by the chemisorbed species.

Keywords Graphene · Graphene oxide · Boron nitride · Boron nitride oxide · Point defects · Molecular simulation

E. Chigo Anota (✉) · A. Escobedo-Morales
Facultad de Ingeniería Química,
Benemérita Universidad Autónoma de Puebla,
Av. San Claudio y 18 Sur,
72570, Puebla, Mexico
e-mail: echigoa@yahoo.es

M. Salazar Villanueva
Facultad de Ingeniería,
Benemérita Universidad Autónoma de Puebla,
Av. San Claudio y 18 Sur,
72570, Puebla, Mexico

O. Vázquez-Cuchillo
Universidad Politécnica Metropolitana de Puebla,
Circuito de las Flores S/N U. Hab. Mateo de Regil,
72464, Puebla, Mexico

E. Rubio Rosas
Centro Universitario de Vinculación,
Benemérita Universidad Autónoma de Puebla,
CP 72570, Puebla, Puebla, Mexico

Introduction

Since Geim and co-workers [1] reported the isolation of a carbon monoatomic layer in 2004, scientific research on nanostructured two-dimensional (2D) systems has increased noticeably. Because of their novel physical and chemical properties, such materials have been recognized as potential materials with which to build data storage systems [2], electronic devices [3], transparent displays [4], chemical sensors, catalyzers [5, 6], and templates [7], among others applications. In this regard, much effort has been focused on developing easy, reliable and simple techniques to obtain stable monoatomic layers [8].

In order to manipulate the physical and chemical properties of monoatomic layers, approaches involving chemical modifications have been explored. For example, it is well known that chemisorption of the hydroxyl group, carboxylic groups and oxygen atoms on the surface of graphene layers results in the formation of a new material: so-called graphene oxide. This material has a bulk modulus higher than other low-dimensional systems based on vermiculite [9], single-walled carbon nanotubes [10], and even graphene [11]. The synthesis through chemical modification of other carbon-based two-dimensional (2D) materials, like graphane [12–14], graphone [15, 16], graphene oxide [17], graphanol [18], and fluorographene [19, 20], has also been reported.

Theoretical calculations of C_nH_m-like models have been used to study the physical and chemical properties of graphene [21], graphene oxide [22], III-A nitrides [23], and silicon carbide sheets [24]. For example, Chigo et al. [22] reported first principles calculations dealing with the effect on its physical properties of chemical modification of graphene oxide using molecular models [$C_{54}H_{17}$+$(OH)_3$+O +COOH]. They found that upon removing the carboxyl group –COOH, a transition semimetal-semiconductor occurs/happens/results. Similar molecular models have also been used to explore the adsorption of water [25] and the feasibility of obtaining stable Li- and F-doped hexagonal boron nitride sheets [26].

Although it is well established that the elemental composition largely determines the resulting physical properties of materials, formation of structural defects can also modify them. This holds also for nanosized systems, in which their influence is notoriously enhanced. Therefore, knowledge of the effect of structural defects on the physical properties of low-dimensional materials is highly desirable [27]. In this regard, while detailed studies of defects in carbon-based monoatomic layers using electron and probe microscopies exist [28–30], theoretical studies that help understand the influence of such defects on the structural stability and the resulting physical properties are still scarce [31].

Here, we present a theoretical-computational study of the influence of point defects on the structural and electronic properties of graphene, graphene oxide, hexagonal boron nitride, and boron nitride oxide sheets. The influence of point defects on the atomic array, bond length, dipole moment, binding energy, and HOMO–LUMO energy gap was analyzed.

Computational methodology

The physical properties of the studied 2D structures were calculated using the DMOL^3 Quantum Chemistry code [32] based on density functional theory (DFT) [33–36] at the level of local density approximation (LDA). Perdew-Wang [37] parameterization was applied for the exchange-correlation term, and the core electrons were modeled using a double numeric polarized atomic base (DNP) [38, 39]; further details can be found elsewhere [21–26]. The cutoff orbital length and the tolerance for the self-consistent field (SCF) cycle were set as 0.40 nm and 1.0×10^{-6} Ha, respectively. The condition of non-complex frequencies was established as the stability criterion for the studied systems [40]. All the models were electrically neutral. While circular geometries were chosen to avoid undesirable effects induced due to anisotropy, the system-size was determined by the convergence of cohesion energy ($\Delta E\approx10^{-3}$ Ha).

The optimized molecular models used to simulate graphene (G; $C_{54}H_{18}$), graphene oxide [GO; $C_{54}H_{17}$+$(OH)_3$ +O+COOH], hexagonal boron nitride (hBN; $B_{27}N_{27}H_{18}$), and boron nitride oxide [BNO; $N_{27}B_{27}H_{17}$+$(OH)_3$+O +COOH] sheets are shown in Fig. 1. Two different configurations of the boron nitride oxide sheet were modeled, considering the nature of the atoms bonded with the chemisorbed species: (1) when most are nitrogen atoms (BNO/A_1), and (2) when most are boron atoms (BNO/A_2).

Results and discussion

Systems without structural defects

The optimized graphene (G) sheet shows a planar surface (Fig. 1a) constituted by an array of hexagonal sub-units. The calculated C–C bond length for the inner hexagons was 1.41 Å, in agreement with the characteristic interatomic distance reported for sp^2 carbon bonds [20, 41]. In the case of graphene oxide (GO) (Fig. 1b), the chemical interaction of the carbon sheet with the –OH, –COOH and O species induces a slight distortion of the hexagonal sub-units, bending the layer. This effect is probably due to the formation of sp^3-like orbitals, as the disposition of the new interatomic bonds indicates. It is worth noting that the binding energy of the GO sheet (21.13 eV) is slightly larger than that calculated for G layer (19.18 eV), suggesting the possibility of obtaining stable graphene oxide sheets directly from the oxidation of graphene.

Although the main structural features of the G and GO sheets are quite similar, their electronic properties differ considerably. The calculated bond lengths and binding energies for the G and GO molecular models are summarized in Table 1.

Figure 1(c–e) shows the optimized models for hexagonal boron nitride sheet (hBN) and the two different configurations of boron nitride oxide sheet (BNO/A_1 and BNO/A_2). It can be seen that the hBN sheet has a planar topography constituted by a hexagonal array of B and N atoms joined by covalent sp^2 bonds. Like G, the incorporation of hydroxyl, carboxyl and epoxy groups bends the hBN sheet slightly. This is attributed to some displacement of charge towards chemisorption sites, which in turn modifies the bond strength of the surrounding atoms. Table 2 lists the structural features of the hBN and BNO systems.

Estimation of the dipole moment (p) of chemical systems can provide a global insight into their capacity to interact with another molecule or chemical complexes when local ionization energy surfaces capable of revealing the actual reactive sites are not available [42]. The calculated dipole moments for the G and hBN sheets were 2.9×10^{-3} and 13.4×10^{-3} D, respectively, revealing the polar character of

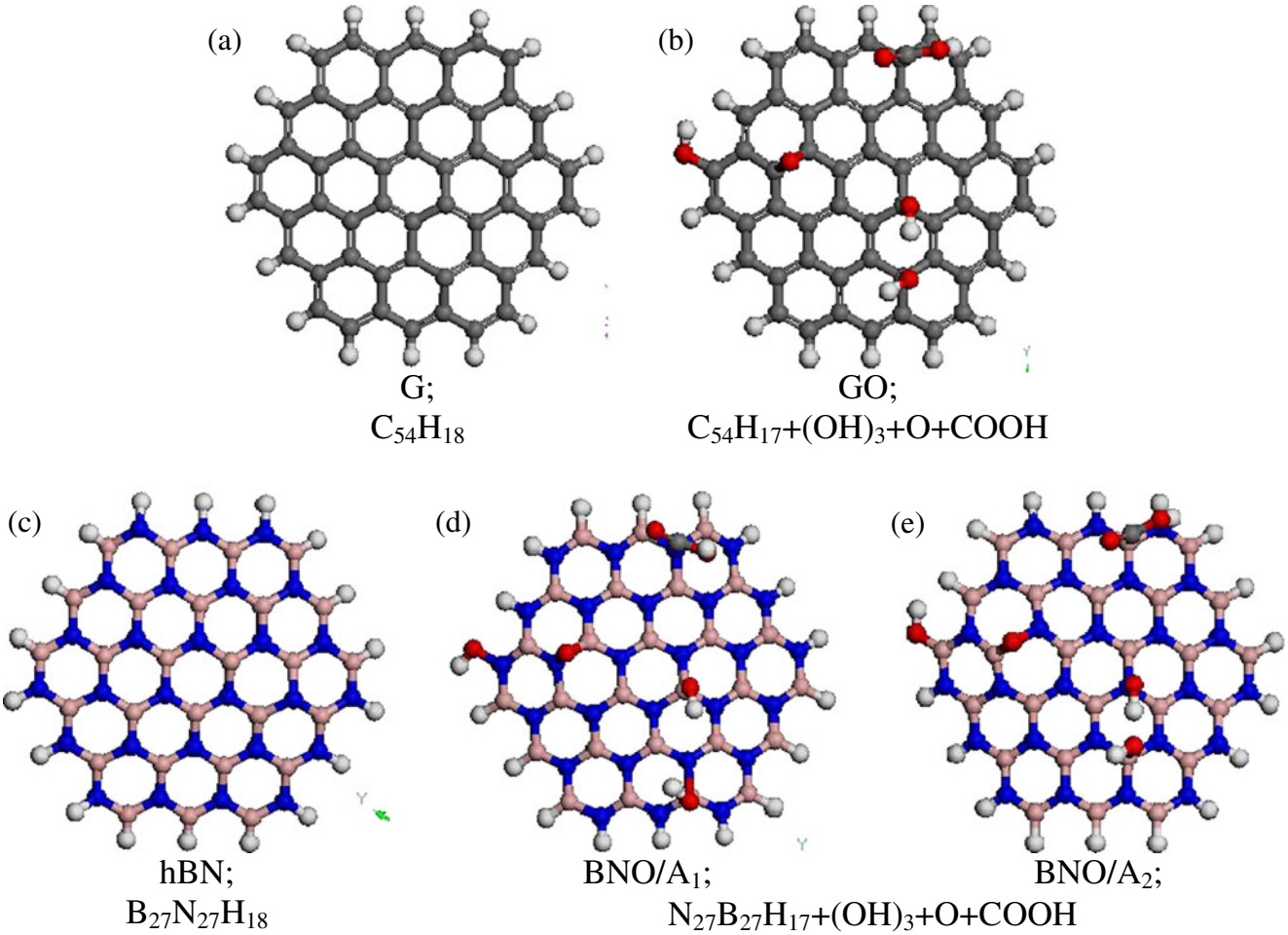

Fig. 1 Appearance of the optimized models of **a** graphene; **b** graphene oxide; **c** hexagonal boron nitride; and **d**, **e** boron nitride oxide sheets. *Gray* Carbon, *white* hydrogen, *red* oxygen, *blue* nitrogen, *pink* boron

both systems; nevertheless, such low magnitudes indicate that they interact weakly through dipole–dipole attraction with stronger polar molecules like water ($p_{H_2O} = 1.85$ D) [43]. Alem et al. [44] were able to demonstrate experimentally the polar character of hBN layers. Previous DFT calculations of smaller G ($C_{24}H_{12}$) and hBN ($B_{12}N_{12}H_{12}$) 2D models [21] also estimated the magnitude of the dipole moment for both systems at around ~10^{-3} D, supporting the validity of molecular models to study the polar character of larger layers.

In the case of GO, a substantive difference of its dipole moment respect to the G sheet (>2,000 %) was observed.

Table 1 Bond lengths, dipolar moment, HOMO–LUMO energy gap and binding energy calculated for the graphene (G) and graphene oxide (GO) systems. V_C Carbon vacancy, N_C substitutional nitrogen

System	Bond length (Å)					Binding energy (eV)	Dipole moment (10^{-3} D)	HOMO-LUMO energy gap (eV)
	C–C	C–H	O–H	C–COOH	C–N			
G	1.41 1.41[a] 1.407[b]	1.10	–	–	–	19.18	2.9	1.94
G+V_C	1.39–1.45	1.10	–	–	–	18.57	1055.0	0.11
G+N_C	1.41	1.09	–	–	1.39	19.04	1374.4	1.69
GO	1.41–1.50	1.10	0.97	1.61	–	21.13	6470.0	0.42
GO+V_C	1.37–1.77	1.09	0.98	1.58	–	20.61	5970.0	0.52
GO+N_C	1.41	1.09	0.98	1.59	1.38	21.02	6427.8	0.26

[a][20]
[b][41]

Table 2 Bond lengths, dipolar moment, HOMO–LUMO energy gap and binding energy calculated for the hexagonal boron nitride (hBN) and boron nitride oxide (BNO) systems. V_N Nitrogen vacancy, V_B boron vacancy, C_N substitutional carbon in nitrogen site, C_B substitutional carbon in boron site

System	Bond length (Å)							Binding energy (eV)	Dipole moment (10^{-3} D)	HOMO–LUMO energy gap (eV)
	B–N	B–H	N–H	O–H	X–COOH	C–N	C–B			
BN	1.44	1.21	1.02	–	–	–	–	17.16	13.4	4.84
	1.44[a]									4.64[c]
	1.44[b]									
$BN+V_N$	1.43	1.21	1.02	–	–	–	–	16.50	835.9	2.00
$BN+V_B$	1.43	1.21	1.02	–	–	–	–	16.51	184.6	0.36
$BN+C_N$	1.44	1.21	1.02	–	–	–	1.50	17.09	221.2	3.60
$BN+C_B$	1.44	1.21	1.02	–	–	1.39	–	17.07	234.9	0.56
BNO/A_1	1.43–1.47	1.21	1.02	0.97	3.48	–	–	18.76	15840.0	1.20
BNO/A_1+V_N	1.32–1.45	1.21	1.02	0.97	1.62	–	–	18.44	7340.0	1.42
BNO/A_1+V_B	1.42–1.44	1.21	1.02	0.97	1.42	–	–	18.44	9309.8	2.82
BNO/A_1+C_N	1.45	1.21	1.02	0.97	1.54	–	1.36	18.75	19655.4	0.54
BNO/A_1+C_B	1.43	1.21	1.02	0.97	1.64	1.36	–	18.88	6973.5	1.73
BNO/A_2	1.44–1.45	1.21	1.02	0.97	1.88	–	–	18.88	6558.3	2.25
BNO/A_2+V_N	1.43–1.45	1.21	1.02	0.98	1.48	–	–	18.29	15430.8	0.46
BNO/A_2+V_B	1.41–1.42	1.21	1.02	0.98	1.40	–	–	18.45	9304.0	3.06
BNO/A_2+C_N	1.44	1.21	1.02	0.98	3.11	–	1.50	18.88	15353.8	1.78
BNO/A_2+C_B	1.44–1.46	1.20	1.02	0.97	1.54	1.36	–	18.76	19655.4	0.54

[a][23]
[b][47]
[c][48] (theoretical study)

The strong polar character of GO ($p_{GO} = 6.47$ D) is attributed to the formation of large charge densities around the chemisorbed hydroxyl groups. Analogous behavior is observed for the BNO/A_1 and BNO/A_2 models, with dipole moments of 15.84 and 6.55 D, respectively. These results suggest that the polar character of BNO layers might be controlled by a selective process of the chemisorbed species along with the atomic sites where chemisorption takes place.

The chemical reactivity of molecular systems is associated closely with the HOMO–LUMO energy gap (difference between the energies of the lowest unoccupied molecular orbital and the highest occupied molecular orbital). This relevant feature was calculated for each system. The calculated energy gap of the GO sheet was 0.42 eV, which is considerably lower than that of the G model (1.94 eV) [22]. This indicates that a semiconductor–semimetal transition could occur when graphene is oxidized.

For the case of the BNO/A_1 and BNO/A_2 models, the calculated energy gaps fall in the range of semiconductor behavior, 1.20 and 2.25 eV, respectively. Comparing with the hBN sheet, it is observed that, in general, its energy gap decreases when it is oxidized. The notorious difference between the calculated energy gaps of BNO models suggests that their electronic properties depend strongly on the atomic sites to which the oxidant species become bonded.

Tables 1 and 2 summarize the calculated dipole moment and HOMO–LUMO energy gap for each carbon- and hBN-based system, respectively.

Defects in graphene and graphene oxide

Figure 2 shows the optimized models of the G and GO sheets containing structural defects. It was found that if a carbon vacancy (V_C) is introduced into the graphene model the atoms around it tend to reorganize, forming a pentagon and two open rings (see Fig. 2a). It is proposed that an increase in total energy due to the introduction of dangling bonds makes the system reconstruct itself. However, it is expected that local stress remains near the point defect. On the other hand, incorporation of a substitutional nitrogen (N_C) does not lead to any reconstruction (Fig. 2b). The similarity between the atomic radii of N and C atoms, along with the formation of sp^2 bonds, prevent a large distortion of the system. Since the electronegativity of nitrogen is larger than that of carbon (3.2 and 2.7, respectively [45]), the carbon atoms surrounding the substitutional nitrogen approach each other slightly, probably inducing lattice strain. Nevertheless, as the N–C bond length suggests (1.39 Å), the induced strain must be small and distributed symmetrically around the N_C defect, allowing the nitrogen-doped graphene sheet to be stable.

The optimized model of the GO sheet containing a single carbon vacancy is shown in Fig. 2c. It was found that, after introducing a V_C in the GO system, a full reconstruction of two carbon rings from hexagonal to pentagonal geometry occurs, suggesting that the chemical interaction of carbon atoms near the structural defect with chemisorbed groups is responsible for allowing the formation of such pentagonal subunits. It is worth noting that the introduction of a V_C has a stronger effect on the GO than on the G sheet.

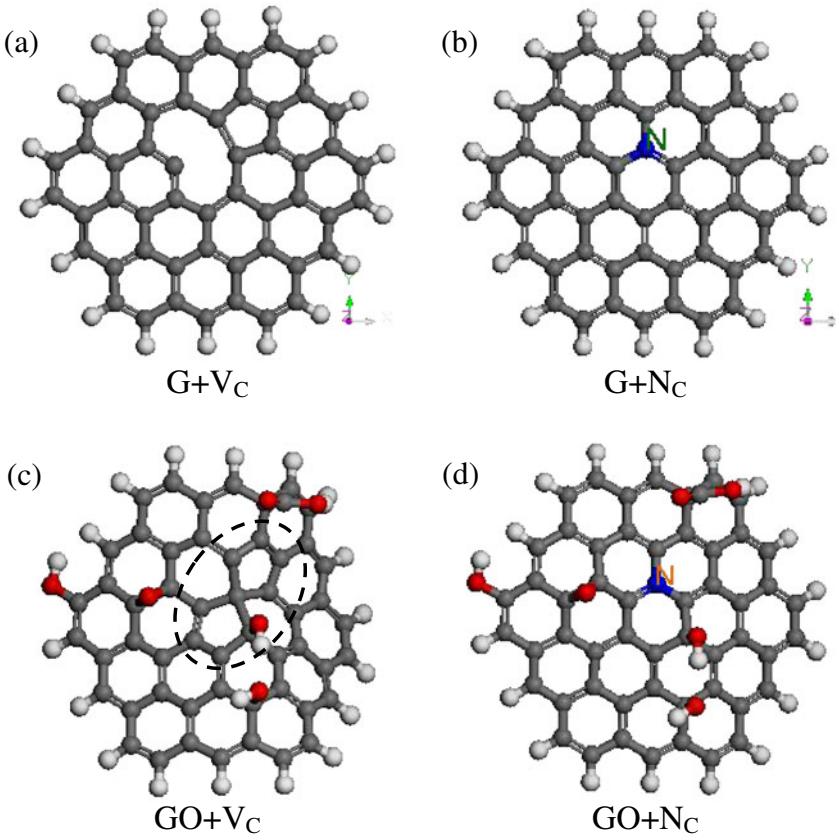

Fig. 2 Optimized models of graphene (**a**, **b**) and graphene oxide (**c**, **d**) containing structural defects. V_C Carbon vacancy, N_C substitutional nitrogen. *Gray* Carbon, *white* hydrogen, *red* oxygen, *blue* nitrogen. *Ellipse* Pentagonal sub-units formed after reconstruction process of the GO sheet containing a V_C defect

Like the nitrogen-doped graphene sheet, incorporation of a substitutional nitrogen into the graphene oxide model does not destabilize the system, or introduce a large structural distortion; the same reasons concerning atomic radii and sp^2 hybridization are believed to be responsible.

Based on the analysis of our 2D carbon-based systems, it is proposed that preferential doping elements to obtain stable doped G and GO should fulfill the following requirements: (1) a similar atomic radius as the substituted atom in order to minimize lattice strain and to prevent severe reconstruction processes; (2) electronegativity of around 2.5, so that sites with large charge density capable of destabilizing the system can be avoided; and (3) the capacity to establish sp^2-like bonds, otherwise the system could be forced to remove the dangling bonds by chemisorption or through reconstruction processes.

The effect of point defects on the resulting physical properties involves not only structural issues; perturbation of the atomic array could also lead to significant changes of the dipole moment and energy gap. In this regard, it was found that when a V_C is introduced into the G sheet, the permanent dipole moment increases from 2.9×10^{-3} to 1.05 D, and a N_C defect increases it even further (1.37 D). For the GO model, the influence of the structural defects on the dipole moment is not as dramatic as for G, which can be attributed to the fact that charge located at the chemisorption sites cannot be redistributed easily. On the other hand, it was determined that a transition from semiconductor to semimetal behavior occurs when either a V_C or a N_C defect is generated in the graphene model. It is interesting to note that such a transition was not observed for molecular models of graphene if the central carbon-ring is substituted entirely by nitrogen atoms ($C_{18}N_6H_{12}$) [21]. Moreover, Panchakarla et al. [46] reported that heavy nitrogen doping of graphene sheets does not results in semimetal behavior. Therefore, it seems reasonable to propose that the level of nitrogen doping has a strong effect on the value of the energy gap of doped graphene layers. In the case of the GO sheet, although formation of a point defect (V_C or N_C) modifies the energy gap slightly, no transition in electronic behavior was observed.

Table 1 presents the calculated dipole moment and HOMO–LUMO energy gap for the modeled graphene and graphene oxide systems containing structural defects.

Defects in boron nitride and boron nitride oxide

The optimized hBN sheets containing structural defects are shown in Fig. 3. It was found that the hBN system remains stable after the formation of a vacancy-type defect; nevertheless, the resulting consequence depends on the nature of the removed atom. While a nitrogen vacancy (V_N) tends to bend the hBN sheet (Fig. 3a), the formation of a boron vacancy (V_B) does not disturb the planar topography (Fig. 3b). Although the binding energy of the hBN sheet with a V_N defect is similar to that containing a V_B defect (see Table 2), the

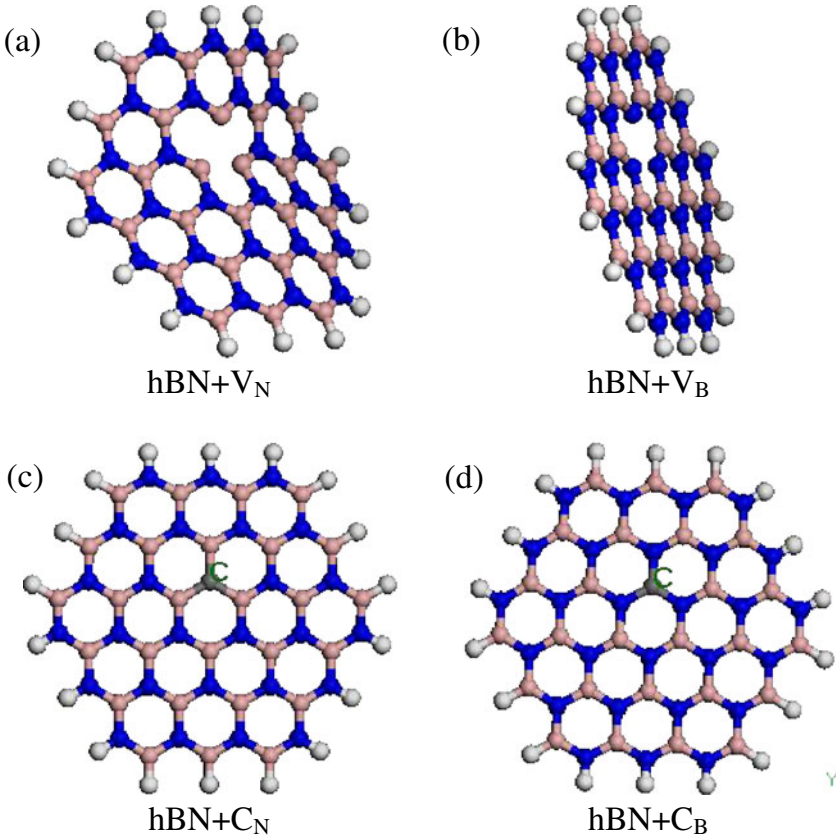

Fig. 3 Optimized models of hexagonal boron nitride (hBN) sheets containing different structural defects. **a** Nitrogen vacancy, **b** boron vacancy, **c** substitutional carbon in nitrogen site, **d** substitutional carbon in boron site. *Gray* Carbon, *white* hydrogen, *blue* nitrogen, *pink* boron

induced lattice distortion suggests that V_N is the least energetically favorable vacancy-type defect.

Figure 3(c,d) shows the optimized carbon doped hBN models. It can be seen that carbon doping results in a non-distorted stable doped hBN sheet, regardless of whether carbon substitutes nitrogen or boron.

Like the hBN system, incorporation of a point defect (vacancy or substitutional) into the BNO sheets does not lead to structural instability (Figs. 4, 5). A comparison between the BNO/A_1 and BNO/A_2 models containing structural defects suggests that the distortion induced by the vacancy-type defects depends on the relative positions of the point defect and the chemisorbed species (see Figs. 4a,b and 5a,b). For example, while the formation of dangling bonds generated due to a V_N defect does not activate a severe reconstruction process, the system removes them by building a pentagonal subunit when a V_B defect is present. It is interesting to note for the BNO/A_1 model that the lattice distortion induced by the point defect allows chemical interaction between the chemisorbed hydroxyl groups, leading to the formation of molecular water (Fig. 4a).

The defect-free hBN sheet had a lower dipole moment (13.4×10^{-3} D) than analogous systems containing a point defect. In this regard, it was found that the formation of a V_B or V_N defect increases the magnitude of the dipole moment to 184.6×10^{-3} and 835.9×10^{-3} D, respectively. Not only the formation of point defects determines the resulting dipolar moment of the hBN sheet, the oxidation process also noticeably changes its magnitude. For example, 15.84 and 6.55 D were calculated for the BNO/A_1 and BNO/A_2 configurations, respectively, i.e., more than one order of magnitude more than hBN sheet. A comparison among the calculated dipolar moment of the hBN and BNO sheets with and without point defects suggests that the polar character of the system can be increased by introducing lattice disorder; nevertheless, the overall effect depends on the nature and spatial distribution of the structural defects (see Table 2).

For the hBN sheet model, it was found that formation of a V_B leads to a semiconductor–semimetal transition, although a comparable effect was not achieved by incorporating a V_N defect. Analogous behavior was observed in carbon-doped hBN sheets. Therefore, it seems that the energy gap of hBN sheets is more sensitive to perturbations of the boron sub-lattice than those related to the nitrogen sub-lattice.

Like the hBN system, the incorporation of a point defect has a drastic effect on the energy gap of BNO sheets. For example, the formation of a V_B defect increases the energy gap of the BNO/A_1 model (3.06 eV) and the incorporation of a substitutional carbon (C_B) in the BNO/A_2 model results in a semiconductor–semimetal transition. However, it is important to point that, unlike hBN, no general tendency was recognized.

Table 2 summarizes the calculated HOMO–LUMO energy gap for the BN and BNO models containing point defects.

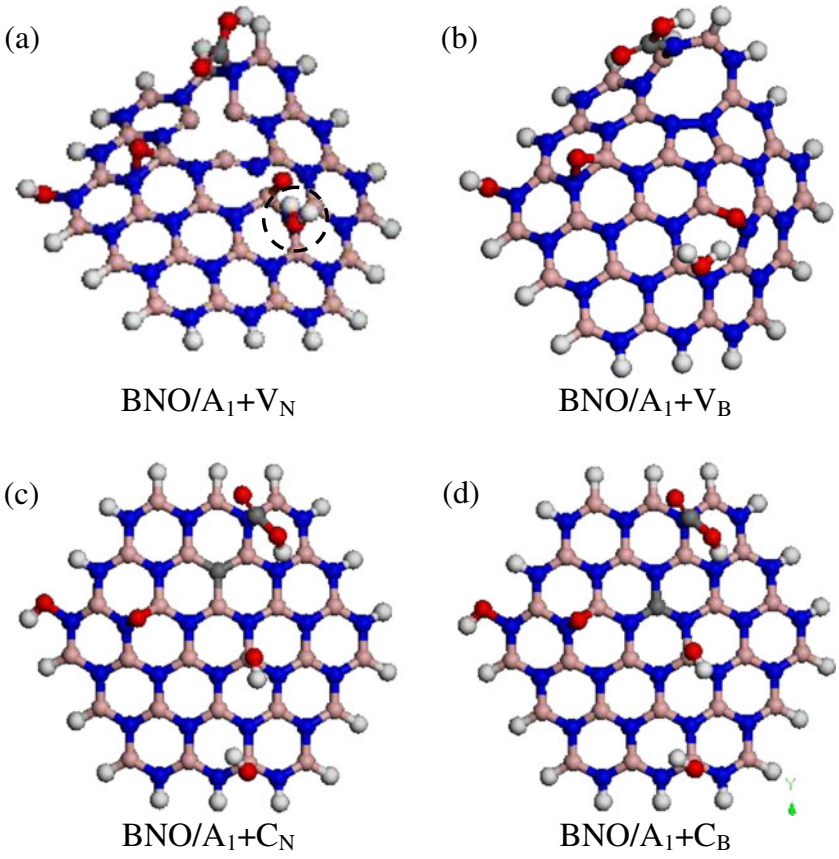

Fig. 4 Optimized models of boron nitride oxide sheets (configuration BNO/A_1) containing different structural defects. **a** Nitrogen vacancy, **b** boron vacancy, **c** substitutional carbon in nitrogen site, **d** substitutional carbon in boron site. *Gray* Carbon, *white* hydrogen, *blue* nitrogen, *pink* boron. *Circle* Molecular water formed by chemical interaction of hydroxyl groups on the surface of the BNO/A_1 sheet

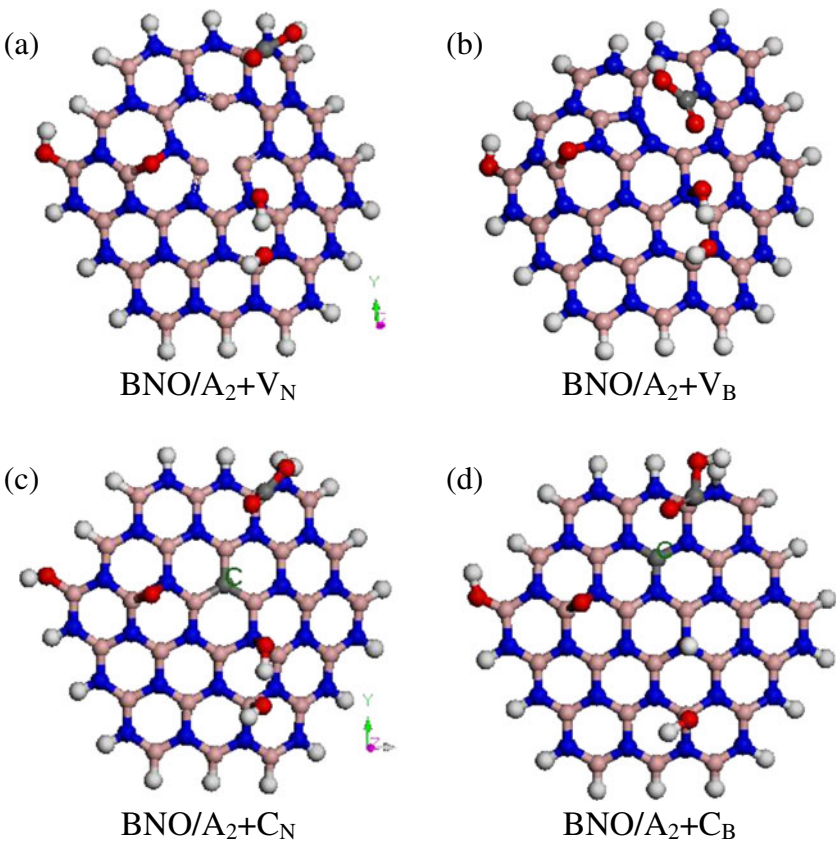

Fig. 5 Optimized models of boron nitride oxide sheets (configuration BNO/A_2) containing different structural defects. **a** Nitrogen vacancy, **b** boron vacancy, **c** substitutional carbon in nitrogen site, **d** substitutional carbon in boron site. *Gray* Carbon, *white* hydrogen, *blue* nitrogen, *pink* boron

Conclusions

The results obtained indicate that incorporation of point defects into graphene, graphene oxide, hexagonal boron nitride and boron nitride oxide sheets does not necessarily result in structural instability; however, surface distortions and reconstruction processes can be generated, mainly when a vacancy-type defect is involved.

On concerning the cohesion of the studied systems a general tendency is observed: the formation of vacancy-type defects reduces the binding energy to a larger extent than substitutional atoms. For the hBN and BNO models, although neither a vacancy-type defect nor carbon doping leads to structural instability, it is proposed that among them the V_N is the least energetically favorable defect.

Finally, it is concluded that the formation of point defects in graphene, graphene oxide, hexagonal boron nitride and boron nitride oxide sheets has a strong effect on their structural and electronic properties; therefore, taking advantage from this fact, development of methods that allow us to control the nature and density of structural defects could lead to potential novel applications of these monoatomic layered materials.

Acknowledgments This work was supported partially by Vicerrectoría de Investigación y Estudios de Posgrado de la Benemérita Universidad Autónoma de Puebla (VIEP-BUAP; grant # CHAE-ING12-G) and Consejo Nacional de Ciencia y Tecnología (CONACyT-Mexico; grants # 0083982 & CB2011/168027).

References

1. Novoselov KS, Jiang D, Schedin F, Booth TJ, Khotkevich VV, Morozov SV, Geim AK (2005) Proc Natl Acad Sci USA 102 (30):10451–10453
2. Serrano J, Bosak A, Arenal R, Krisch M, Watanabe K, Taniguchi T, Kanda H, Rubio A, Wirtz L (2007) Phys Rev Lett 98 (9):095503–095504
3. Soldano C, Mahmood A, Dujardin E (2010) Carbon 48(8):2127–2150
4. Bonaccorso F, Sun Z, Hasan T, Ferrari AC (2010) Nat Phot 4:611–622
5. Rangel NL, Seminario JM (2008) J Phys Chem A 112 (51):13699–13705
6. Allen MJ, Tung VC, Kaner RB (2010) Chem Rev 110(1):132–145
7. Oida S, McFeely FR, Hannon JB, Tromp RM, Copel M, Chen Z, Sun Y, Farmer DB, Yurkas J (2010) Phys Rev B 82(4):041411(1)–041411(4)
8. Ping Loh K, Bao Q, Kailian P, Yang A, Yang J (2010) J Mat Chem 20:2277–2289
9. Ballard DGH, Rideal GR (1983) J Mater Sci 18(2):545–561
10. Sumio I, Ichihashi T (1993) Nature 363:603–605
11. Novoselov KS, Geim AK, Morozov SV, Jiang D, Zhang Y, Dubonos SV, Grigorieva IV, Firsov AA (2004) Science 306:666–669
12. Sofo JO, Chaudhari AS, Barber GD (2007) Phys Rev B 75 (15):153401–153404
13. Elias DC, Nair RR, Mohiuddin TMG, Morozov SV, Blake P, Halsall MP, Ferrari AC, Boukhvalov DW, Katsnelson MI, Geim AK, Novoselov KS (2009) Science 323:610–613
14. Bhattacharya A, Bhattacharya S, Majumder C, Das GP (2011) Phys Rev B 83(3):033404
15. Zhou J, Wang Q, Sun Q, Chen XS, Kawazoe Y, Jena P, Zhou J, Wang Q, Sun Q, Chen XS, Kawazoe Y, Jena P (2009) Nano Lett 9 (11):3867–3870
16. Xiang H, Kan E, Wei SH, Whangbo MH, Yang J (2009) Nano Lett 9(12):4025–4030
17. Dikin DA, Stankovich S, Zimney EJ, Piner RD, Dommett GHB, Evmenenko G, Nguyen ST, Ruoff RS (2007) Nature 448:457–460
18. Wang WL, Kaxiras E (2010) New J Phys 12:125012
19. Nair RR, Ren W, Jalil R, Riaz I, Kravets VG, Britnell L, Blake P, Schedin F, Mayorov AS, Yuan S, Katsnelson MI, Cheng HM, Strupinski W, Bulusheva LG, Okotrub AV, Grigorieva IV, Grigorenko AN, Novoselov KS, Geim AK (2010) Smal 6(24):2877–2884
20. Nava Contreras C, Chigo Anota E, Hernández Cocoletzi H (2011) J Mol Model 17(8):2093–2097
21. Chigo Anota E (2009) Sup y Vac 22(1):19–23
22. Hernández Rosas JJ, Ramírez Gutiérrez RE, Escobedo Morales A, Chigo Anota E (2011) J Mol Model 17(5):1133–1139
23. Chigo Anota E, Salazar Villanueva M, Hernández Cocoletzi H (2010) Phys Stat Solidi (c) 7(7):2252–2254
24. Chigo Anota E, Hernández Cocoletzi H, Bautista Hernández A, Sánchez Ramírez JF (2011) J Comput Theor Nanosci 8(4):637–641
25. Chigo Anota E, Salazar Villanueva M (2009) Sup y Vac 22 (2):23–28
26. Chigo Anota E, Salazar Villanueva M, Hernández Cocoletzi H (2010) Phys Stat Solidi (c) 7(10):2559–2561
27. Lin Y, Williams TF, Cao W, Elsayed-Ali HE, Connell JW (2010) J Phys Chem C 114(41):17434–17439
28. Gass MH, Bangert U, Bleloch AL, Wang P, Nair RR, Geim AK (2008) Nat Nanotechnol 3:676–686
29. Meyer JC, Kisielowski C, Erni R, Rossell MD, Crommie MF, Zettl A (2008) Nano Lett 8(11):3582–3586
30. Ugeda MM, Brihuega I, Guinea F, Gómez Rodríguez JM (2010) Phys Rev Lett 104(9):096804
31. Bagri A, Mattevi C, Acik M, Chabal YJ, Chhowalla M, Shenoy VB (2010) Nat Chem 2:581–587
32. Delley B (1990) J Chem Phys 92(1):508–517
33. Kohn W, Becke AD, Parr RG (1996) J Phys Chem 100 (31):12974–12980
34. Jones RO, Gunnarsson O (1989) Rev Modern Phys 61(3):689–746
35. Kohn W (1999) Rev Mod Phys 71(5):1253–1266
36. Chigo Anota E, Rivas Silva JF (2005) Rev Col Fís 37(2):405–417
37. Perdew JP, Wang Y (1992) Phys Rev B 45(13):13244–13249
38. Delley B (1996) J Phys Chem 100(15):6107–6110
39. Delley B (2000) J Chem Phys 113(18):7756–7764
40. Foresman JB, Frisch Æ (1996) Exploring chemistry with electronic structure methods, vol 70, 2nd edn. Gaussian, Pittsburgh, PA
41. Maslov MM, Podlivaev AI, Openov LA (2009) Phys Lett A 373:1653
42. Dinadayalane TC, Murray JS, Concha MC, Politzer P, Leszczynski J (2010) J Chem Theory Comput 6(4):1351–1357
43. Lovas FJ (1978) J Phys Chem Ref Data 7:1445–1751
44. Alem N, Erni R, Kisielowski C, Rossell MD, Gannett W, Zettl A (2009) Phys Rev B 80(15):155425
45. Sanderson RT (1983) J Am Chem Soc 105(8):2259–2261
46. Panchakarla LS, Subrahmanyam KS, Saha A, Govindaraj A, Krishnamurthy HR, Waghmare UV, Rao CNR (2009) Adv Mat 21(46):4726–4730
47. Pakdel A, Zhi C, Bando Y, Golberg D (2012) Materials Today 15:256–265
48. Topsakal M, Aktürk E, Ciraci S (2009) Phys Rev B 79:115442